Observation of the spin isovector monopole resonance using the Pb($\vec{p},\vec{n}$)Bi reaction at 795 MeV

D. L. Prout,[1,*] J. Rapaport,[2] E. Sugarbaker,[1] D. Cooper,[1,†] S. Delucia,[1] B. Luther,[1,‡] C. D. Goodman,[5] B. K. Park,[4,§] L. Rybarcyk,[3] T. N. Taddeucci,[3] and J. Ullmann[3]

[1]*The Ohio State University, Columbus, Ohio 43210*

[2]*Ohio University, Athens, Ohio 45701*

[3]*Los Alamos National Laboratory, Los Alamos, New Mexico 87545*

[4]*New Mexico State University, Las Cruces, New Mexico 88003*

[5]*Indiana University Cyclotron Facility, Bloomington, Indiana 47405*

(Received 9 June 2000; published 18 December 2000)

We examine a broad resonance in the 0° ^{208}Pb$(p,n)^{208}$Bi and ^{90}Zr$(p,n)^{90}$Nb cross section spectra obtained at 795 MeV incident energy that appears at 32 MeV excitation energy in ^{208}Bi and ^{90}Nb. Earlier data taken at 200 MeV incident energy using the same reactions show no evidence for this resonance. We present theoretical results indicating that the spin isovector monopole predicted at this excitation energy is barely excited at 200 MeV while it is strongly excited at the higher energy. To further investigate this structure we have measured the first complete set of polarization-transfer observables for ^{nat}Pb at 0° using the ($\vec{p},\vec{n}$) reaction at 795 MeV. The data show this resonance is predominantly a spin flip $\Delta S=1$ excitation giving strong supporting evidence for assigning this resonance as the spin isovector monopole.

DOI: 10.1103/PhysRevC.63.014603 PACS number(s): 24.30.Cz, 25.40.Kv, 27.60.+j, 27.80.+w

I. INTRODUCTION

The study of giant resonances with hadronic probes has been important for understanding collective phenomena in nuclei. In particular, the (p,n) reaction provides a very selective probe of isovector ($\Delta T=1$) transitions in nuclei and led to the discovery of the giant Gamow-Teller (GT) resonance which dominates the (p,n) spectra at proton energies above 100 MeV [1–3]. Other collective resonances such as the isovector dipole ($\Delta L=1$, $\Delta S=0$) and spin dipole ($\Delta L=1$, $\Delta S=1$) have been observed and studied through multipole decompositions of (p,n) spectra [4].

One of the most elusive of the predicted collective modes in nuclei has been the isovector giant monopole ($\Delta T=1$, $\Delta L=0$) or ''breathing mode'' resonance. Monopole resonances are $\Delta L=0$ excitations of the nucleus connected with the expansion and compression of the nucleus as a whole and occur with the neutrons and protons oscillating either in phase ($\Delta T=0$, isoscalar) or out of phase ($\Delta T=1$, isovector) and can involve spin transfer ($\Delta S=1$) or nonspin transfer ($\Delta S=0$) excitations. These excitations are driven by operators $Q_{01}=\Sigma_i r_i^2 \sigma_i \tau_i$ and $Q_{00}=\Sigma_i r_i^2 \tau_i$ and result in a radial transition density that has a node at the nuclear surface. As discussed in Ref. [5], this characteristic of the transition density results in the monopole being most strongly excited by reactions that probe just the surface of the nucleus and not the interior. Therefore, reactions involving pions and light ions at forward angles have been favored in searches for monopole excitations as opposed to reactions such as (e,e'), (p,p'), and (p,n) which at intermediate energies sample the nuclear interior as well.

The isoscalar nonspin monopole resonance (ISM) ($\Delta T=0$, $\Delta J^\pi=0^+$, $\Delta S=0$) has been observed earlier using the (^{4}He,^{4}He$'$) reaction [6] and has provided a fundamental nuclear parameter: the nuclear matter compressibility. Reactions involving charge exchange can be used to search for isovector resonances. The isovector nonspin monopole resonance (IVM) can be related to the nuclear polarizability determined from the symmetry energy in the nuclear mass equation [7]. The IVM has been sought for using the (π^+,π^0) reaction and its observation reported by Bowman *et al.* [8]; however, extraction of the IVM resonance parameters, relied heavily on a careful determination of a large background. Recently, confirmation of the existence of the IVM was provided in Ref. [9] by use of the ^{60}Ni(^{7}Li,^{7}Be)^{60}Co reaction.

Evidence for excitation of the spin isovector monopole (SIVM) using the ^{208}Pb$(n,p)^{208}$Ti has been reported [10]. The signal for the SIVM was extracted in a multipole decomposition and sits on a large model dependent background. The signal-to-noise ratio in this experiment was not suitable to make an unambiguous identification of the resonance. Recently, the Pb(^{3}He,tp) reaction at 177 MeV has been measured and provided evidence for the existence of the IVM and SIVM [11]. The strongest evidence for SIVM has been from forward angle (^{3}He,t) data taken on ^{90}Zr at 900 MeV which show a large cross section at the excitation energy expected for the SIVM resonance [12]. This excess cross section is not observed in data taken on the same target with the nominally similar (p,n) reaction at 200 MeV. A recent explanation for this phenomenon has been reported by Auerbach [13]. The (p,n) reaction at this energy probes further into the nuclear interior while the (^{3}He,t) reaction probes mainly the nuclear surface. The spin nature of the

*Present address: DOE Remote Sensing Laboratory, Las Vegas, NV 89115.

†Present address: MIT/Lincoln Laboratory, Lexington, MA 02173.

‡Present address: Concordia College, Moorhead, MN 56562.

§Present address: LANL, Los Alamos, NM 87545.

excitation was assumed from the fact that the driving nucleon-nucleon (NN) interaction is predominantly $\Delta S=1$ at these energies; however, no empirical evidence has previously been reported to determine the spin character of this excitation.

In 1983 Auerbach *et al.* [14] singled out the (p,n) and (n,p) reactions at 800 MeV beam energy as likely candidate reactions for exciting the isovector monopole resonance in heavy nuclei. As the incident proton or neutron energy is raised from 200 to 800 MeV the charge exchange reaction is known to become much more surface peaked in nuclei. Evidence for this comes from nucleon-nucleus elastic scattering which indicates a large increase in the depth of the imaginary part of the optical potential is required in order to describe the data at higher energies (600–800 MeV). The results of detailed calculations for the nonspin isovector monopole in Pb and Zr indicate a factor of two increase in cross section at the higher energy due to the opacity of the nuclear medium. While calculations for the spin monopole were not done, similar arguments apply.

In this article we report on resonances observed at about 32 MeV of excitation energy in ^{90}Nb and Bi excited using the (p,n) reaction at 795 MeV on ^{90}Zr and Pb. This resonance is consistent with the features of the spin isovector monopole resonance as predicted by Auerbach *et al.* [14] and Boucher and Castel [15]. To determine the spin character of the resonance we report on the first *complete* set of polarization-transfer (PT) measurements taken over the giant resonance region using the $(\vec{p},\vec{n})$ reaction at 795 MeV. We also report the first nonspin, spin-transverse, and spin-longitudinal decomposition of the cross sections which can be used to ascertain the magnitude of the contribution of noncentral components to the cross section.

II. CROSS SECTION MEASUREMENTS

A. Experimental method

The data were taken with the Neutron Time-of-Flight (NTOF) Facility at the Los Alamos Meson Physics Facility. The facility has been described in detail in Ref. [16] and the major components consisted of a beam swinger for directing the proton beam at various angles onto the target, a long (200 m) open-air neutron flight path at the end of which is a neutron polarimeter composed of bars of organic scintillation detectors. The neutron polarimeter contained four parallel planes perpendicular to the neutron flight path. The first three planes contained liquid scintillator in ten optically isolated cells with dimensions of $10\times10\times107$ cm^3. The last plane was composed of ten bars of plastic scintillator. A thin plane of plastic scintillation detectors was placed in front of the larger neutron plane detectors to veto charged particles. Another thin plane of plastic scintillator was placed between the front and back planes to tag charged particles created in the front planes. The neutron polarization was determined by measuring the asymmetry in the scattering of neutrons between the front and back planes of the polarimeter. The PT observables D_{NN} and D_{LL} were measured for the $(\vec{p},\vec{n})$ reaction on natural Pb, natural C(98.9% ^{12}C) and CD_2. Differential cross section spectra were measured for Pb (309 mg/cm^2), ^{90}Zr (25.5 mg/cm^2), CD_2, C (358 mg/cm^2), and ^{7}Li (534 mg/cm^2). The proton beam energy was 795 MeV with a beam current between 20 and 40 na and a typical beam polarization of 0.65. This quantity was monitored continuously by two beamline polarimeters. Absolute neutron cross sections were determined by normalizing to the 0° cross section for the ^{7}Li$(p,n)^7$Be(g.s.+0.43) reaction (27 mb/sr in center of mass [17]). The scattering angle was 0° and the neutron flight path was 200 m. Because of the long flight path, the angular acceptance of the detector was only 0.29°. Systematic uncertainties resulting from beam current and target thickness are estimated to be less than 8%. A 3% uncertainty has been associated with the absolute normalization to the ^{7}Li$(p,n)^7$Be reaction [16]. The detector efficiency over the energy range of neutrons detected in the experiment was constant. A discussion concerning the NTOF detector efficiency and extraction of differential cross sections from NTOF data can be found in Ref. [18].

The 200-MeV cross section data for the Pb(p,n)Bi and Zr(p,n)Nb reactions are from neutron time-of-flight measurements made at the Indiana University Cyclotron Facility (IUCF). Details concerning these measurements may be found in the specific references cited. All 200-MeV data were normalized to the ^{7}Li$(p,n)^7$Be(g.s.+0.43) reaction as well for which a constant center-of-mass (c.m.) cross section of 27 mb/sr has been assumed based on arguments set forth in Ref. [17].

B. Discussion of cross section

In Fig. 1, we present double differential cross section spectra versus excitation energy for the the (p,n) reaction on Pb, ^{90}Zr, and C targets at 795 MeV and at 0° scattering angle. Superimposed on these spectra are 200-MeV (p,n) reaction spectra taken on the same targets at 0° scattering angle and normalized to the present data over the first 20 MeV of excitation. The 200-MeV data have been spread with a Gaussian to smear the data and simulate the lower energy resolution of the 795-MeV data. The 200-MeV carbon data were taken from Ref. [19] and the Pb and ^{90}Zr data from Ref. [21].

The reason for comparing the data in this way is because the 200-MeV data have been extensively studied and are known to be dominated by Gamow-Teller (GT) strength at 0° at intermediate energies [1,21–24]. Furthermore, studies of the light targets indicate that the empirical 0° GT differential cross sections remain relatively constant from 120 to 800 MeV [17,25,26]. This is because the strength of the underlying nucleon-nucleon (NN) amplitude corresponding to the $\sigma\tau$ operator does not change much over this energy range. Collected in Table I are center-of-mass (c.m.) cross section data for the (p,n) reaction taken at 160, 200, and 795 MeV for assorted targets indicating the relative constancy of the 0° GT cross section with energy. The similarity of the shape of (p,n) spectra for several energies was particularly noted for the case of the ^{11}B(p,n) reaction in Ref. [27].

At zero degrees, the contribution of the $\Delta S=0$, $\Delta L=0$, $\Delta J^\pi=0^+$ strength is concentrated in a single state, the isobaric analog resonance (IAS) or Fermi transition. In this

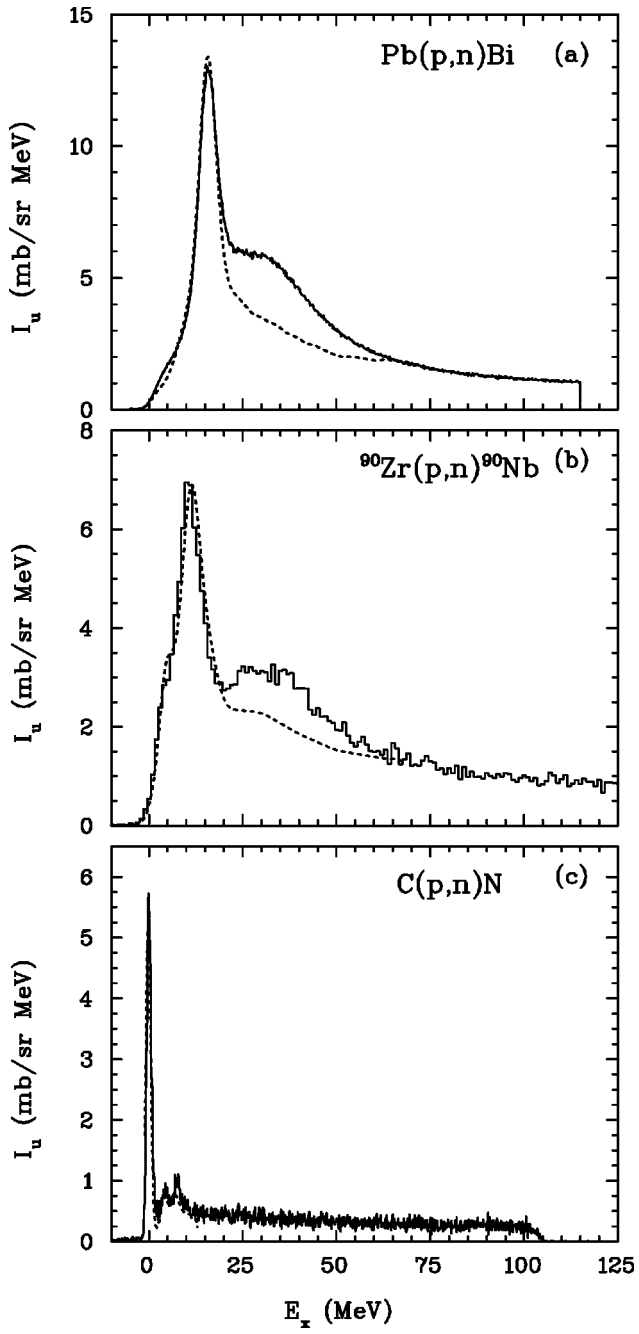

FIG. 1. Shown are spectra as a function of excitation energy for the (a) Pb(p,n), (b) ^{90}Zr(p,n), and (c) ^{12}C(p,n) reactions at 795 MeV. Also shown as a dotted curve are spectra for the same reactions taken at a beam energy of 200 MeV. The 200-MeV data have been normalized to the first 20 MeV of the 795-MeV spectra and spread with a Gaussian function to simulate the poorer resolution of the 795-MeV data.

energy range the Fermi 0° cross section is much smaller than the GT transition, with values 15(5) times smaller than the GT at 200(800) MeV [26]. The results of calculations by Klein and Love [28] describe the 200-MeV ^{90}Zr(p,n) data very well and indicate that 95% of the cross section up to 20 MeV excitation is GT. A similar result has been obtained by Wakasa *et al.* [30], indicating that approximately 67% of the

TABLE I. Integral over the Gamow-Teller (GT) and high excitation region for our Pb and Zr data are shown along with a compilation of GT excitation cross sections for various light targets. The light targets show relatively small changes in the center-of-mass (c.m.) cross section over a large energy range. Also, shown are cross sections for Fermi (IAS) and mixed transitions for a number of targets. The 795-MeV ^{13}C(p,n) and ^{12}C(p,n) data are from Ref. [29]. The data from Ref. [29] were multiplied by 1.8 to account for an incorrect normalization used in that reference (see Ref. [18] for details concerning the two normalization methods used here and in Ref. [29]). The 795-MeV ^{14}C(p,n) data are from Ref. [26]. All the data reported on the discrete state transitions at lower energies are from Ref. [1] except for the ^{13}C(p,n) GT transition cross section which came from Refs. [19,20]. The discrete state transitions were studied at a beam energy of 160 MeV.

E_x range	Target	σ_{795} (mb/sr)	$\sigma_{200,160}$ (mb/sr)
0 − 20	Pb	107	188
20 − 55	Pb	166	190
0 − 20	^{90}Zr	75	105
20 − 55	^{90}Zr	95	91
GT 3.95	^{14}C	15.8 ± 0.8	22.3 ± 1.2
IAS 2.31	^{14}C	2.01 ± 0.19	1.9 ± 0.1
g.s.	^{13}C	3.5 ± 0.5	4.2 ± 0.2
GT 3.51	^{13}C	9.0 ± 0.9	10.5 ± 0.1
GT g.s.	^{12}C	7.6 ± 1.1	6.5 ± 0.6
g.s.	^{7}Li	27.8	27.2 ± 3.1

minimum value of the GT sum rule, $3(N\text{-}Z)=30$, is located in the first 20 MeV of excitation and that approximately another 30% of the GT strength is in the next 30 MeV of excitation. We do not attempt a detailed discussion of the Fermi and GT transitions as was done in Ref. [1] but point out that the Fermi makes up a small portion of the cross section across the entire energy range we study.

We show the carbon data in Fig. 1 to demonstrate that for this light target the cross section shape is identical at the two energies. Only a small rescaling of the 200-MeV date was required to overlay the spectra; the 200-MeV data were multiplied by a factor of 1.17. For the heavier targets the shapes of the spectra at the two energies are very similar up to 20 MeV excitation where after they deviate quite significantly over the next 40 MeV of excitation. The ^{90}Zr data in the region from 0 to 20 MeV consists of two large states of GT strength between which is the IAS. In the present data the states are unresolved. Similarly, in the Pb data there is the well-known IAS which lies just under the GT resonance that dominates the spectrum. In Table I we report the integrated double differential cross section for both Pb and ^{90}Zr targets over the low ''GT'' region and over the higher excitation region.

The heavy targets differ from the carbon and the other light nuclei in that the cross sections at 795 MeV in the ''GT'' regions are approximately $\frac{2}{3}$ of the corresponding region at 200 MeV. The 200-MeV Pb data had to be multiplied by 0.57 and the ^{90}Zr data by 0.71 in order to match the 795-MeV data over this region. A decrease in the cross section for the GT excitations might be expected for these heavy

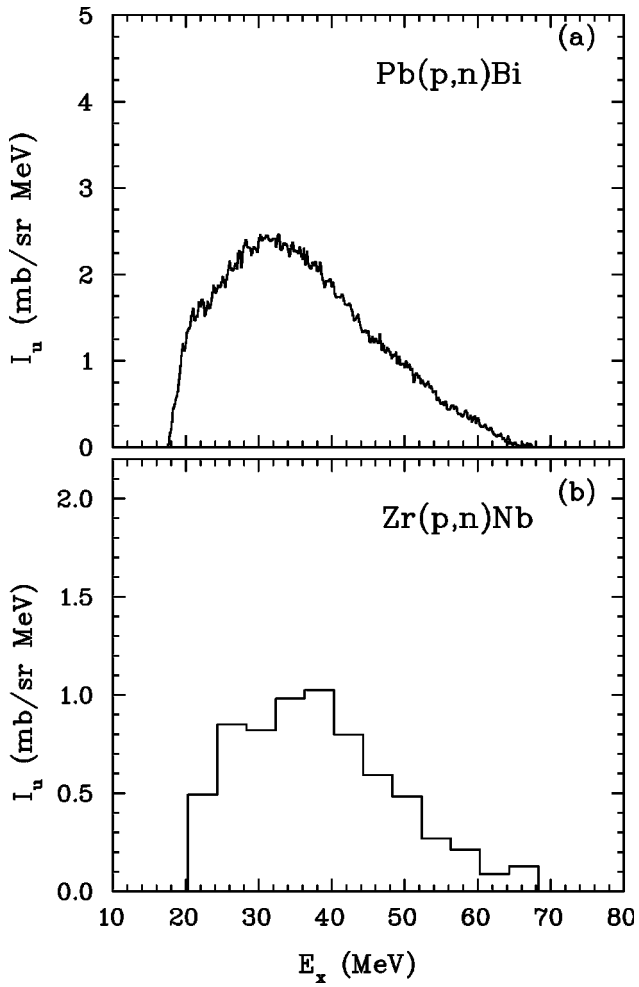

FIG. 2. In the top panel is shown the difference between the 795 MeV excitation spectrum and the scaled 200-MeV spectrum for the ^{nat}Pb(p,n) reaction. In the bottom panel the same procedure was carried out for the ^{90}Zr(p,n) reaction. These spectra provide a rough view of the the position and shape of the excess cross section observed at 795 MeV in these two reactions.

targets due to the depth of the imaginary part of the optical potential. Distorted-waves-impulse-approximation (DWIA) calculations do show a 25% decrease in the cross section of the GT excitation strength for the Zr(p,n) reaction at 795 MeV compared to 200 MeV but for the Pb(p,n) reaction the DWIA results show a similar cross section at 200 and 795 MeV. We do not understand the reasons for the discrepancy between the DWIA calculation and the Pb(p,n) data.

In Fig. 2, we subtract the 200-MeV differential cross section spectrum from the 800 MeV spectrum where the 200-MeV spectrum has been normalized to the low excitation energy region of the 795-MeV data. This has been done to demonstrate how this excess cross section varies with excitation energy as it may reveal the shape of the SIVM. For the Pb(p,n)Bi reaction, the residual cross section is centered at about 32 MeV and is a broad distribution of roughly 25 MeV width (FWHM). The result for Zr is similar to the Pb results but with much poorer statistics. The integral of the differential cross section may be derived from Table I and is about 58 mb/sr for the Pb data and about 30 mb/sr for the Zr data.

III. POLARIZATION OBSERVABLES

A. Experiment and overview

In order to ascertain the spin character of the broad resonance observed in ^{208}Bi at 32 MeV excitation we have measured a complete set of polarization transfer (PT) observables that allow a decomposition of the cross section into $\Delta S=1$ and $\Delta S=0$ partial cross sections. In addition, the $\Delta S=1$ cross section can be separated into spin-transverse and spin-longitudinal partial cross sections which pertain to the strength of the tensor force in the reaction.

The incident proton beam was focused on target after being prepared successively in each of the two spin states, normal $(\hat{N})$, and longitudinal $(\hat{L})$. The average proton polarization was about 0.65. The PT observables D_{NN} and D_{LL}, were measured at 0° for the ^{nat}Pb$(\vec{p},\vec{n})$, C$(\vec{p},\vec{n})$, and ^{2}H$(\vec{p},\vec{n})$ reactions. The ^{2}H observables were determined by subtracting results obtained from the carbon target from those taken on our CD_2 target. Details concerning the extraction of polarization transfer observables as well as the differential cross section at NTOF may be found in Ref. [16].

A formal definition of the expressions we use to extract the partial polarization cross sections from our data is set forth in Refs. [16,31]. These partial cross sections are defined with respect to a set of center-of-mass unit vectors and represent the cross section for flipping the nucleon spin along each of these vectors. The vector $\hat{\boldsymbol{n}}$ is normal to the scattering plane, $\hat{\boldsymbol{q}}$ is in the direction of momentum transfer, and $\hat{\boldsymbol{p}}=\hat{\boldsymbol{q}}\times\hat{\boldsymbol{n}}$. At 0° these partial cross sections may be obtained from the PT observables and the unpolarized cross section (I_u) according to

$$I_0=\frac{1}{4}I_u(1+2D_{NN}+D_{LL}), \tag{1}$$

$$I_q=\frac{1}{4}I_u(1-2D_{NN}+D_{LL}), \tag{2}$$

$$I_p=I_n=\frac{1}{4}I_u(1-D_{LL}), \tag{3}$$

where I_0, I_q, I_p, and I_n correspond to the $\Delta S=0$ spin-independent, $\Delta S=1$ spin-longitudinal, and two spin-transverse partial cross sections, respectively. [These relations can be obtained from Eqs. (12)–(15) in Ref. [16] by setting $\theta_p=\pi/2$.]

Previous articles concerning PT observables using the $(\vec{p},\vec{n})$ reaction at 0° have been limited to a single observable (D_{NN} or D_{LL}) [32,33]. In these articles, the PT observable was examined in the context of the plane-wave-impulse-approximation (PWIA) in order to investigate the strength of the exchange tensor part of the effective nucleon-nucleon (NN) interaction. The PT observable D_{NN} has been used, also, to identify regions of natural $(\Delta J=\Delta L)$ or unnatural parity $(\Delta J=\Delta L\pm 1)$ in the continuum of the ^{90}Zr$(\vec{p},\vec{n})$ reaction at 160 MeV [34].

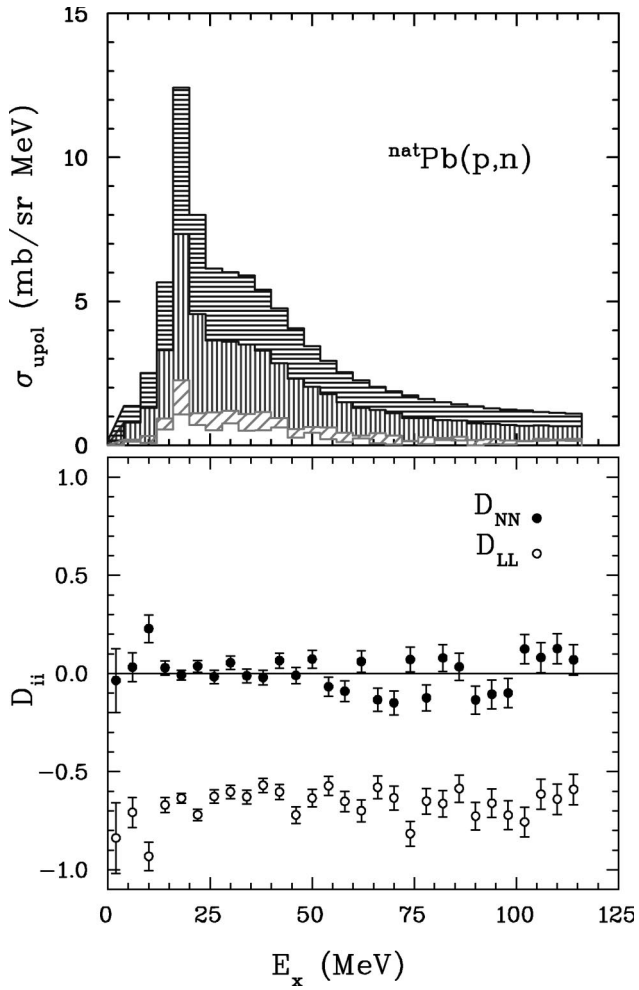

FIG. 3. The top panel shows our 0° cross section data for the Pb(*p*,*n*) reaction. The data for the two spin-transverse (horizontal and vertical lines), spin-longitudinal (diagonal lines), and $\Delta S=0$ (white) partial cross sections are shown. The bottom panel shows the D_{NN} (solid) and D_{LL} (open) results that were used to decompose the cross section. This shows that the strength in the bump at 30–40 MeV energy loss is predominantly from a spin-flip transition.

Because we have measured a complete set of PT observables we are able for the first time to separate unambiguously the non-spin-flip from the spin-flip portions of the cross section. The strength of the exchange tensor part of the nucleon-nucleus interaction is indicated by the difference in the magnitude of the spin-longitudinal and spin-transverse parts of the cross section obtained from the decomposition of the spinflip portion of the cross section. If the exchange tensor strength vanishes the spin-longitudinal and spin-transverse partial cross sections will be identical [32].

B. Results and discussion of polarization observables

The results for the Pb($\vec{p},\vec{n}$) reaction are shown in Fig. 3. The bottom panel shows the measured polarization transfer observables D_{NN} and D_{LL}; while the top panel shows the decomposition of the 0° differential cross section into the two transverse and longitudinal spin components as well as the nonspin component deduced using the above expressions. In the top panel, the areas represented with vertical and horizontal lines correspond to the spin-transverse contributions to the differential cross section and the area with slanted lines is the spin-longitudinal, I_q, contributions. The $\Delta S=0$ strength, I_0, is shown in white. Both I_q and I_0 portions make relatively small contributions to the cross section.

TABLE II. Shown are the values of the polarization observables for all the targets studied in this experiment. These observables were used to calculate the fraction of the cross section that is expected to be spin and nonspin.

Target	D_{NN}	D_{LL}	% $\Delta S=1$	% $\Delta S=0$
^{2}H	-0.119 ± 0.016	-0.760 ± 0.028	100	0
C(g.s.)	-0.091 ± 0.029	-0.877 ± 0.039	100	0
Pb(0–20)	0.020 ± 0.019	-0.673 ± 0.019	91	9
Pb(20–55)	0.014 ± 0.013	-0.637 ± 0.012	90	10
NN(795)	0.034	−0.564	88	12
NN(200)	−0.297	−0.207	95	5

A check that our polarization-transfer measurements are reliable is provided by our data for the ^{2}H($\vec{p},\vec{n}$)2*p* reaction at 0°. The large cross section for this reaction at low excitation energies leads to a $^1S_0$ two proton final state [32,35,36]. This purely ($\Delta L=0$, $\Delta S=1$) transition results since the nonspinflip part of the interaction is Pauli blocked at 0°. Thus, this transition also provides a nominal GT benchmark against which we can compare the data from the Pb($\vec{p},\vec{n}$) reaction. The polarization transfer observables measured for ^{2}H are $D_{NN}=-0.119\pm0.016$ and $D_{LL}=-0.760\pm0.036$. Within uncertainties the value of I_0 is zero, as expected. Our D_{LL} data are consistent with an independent measurement reported by Mercer *et al.* [32]. The measurements [32] for the ^{2}H($\vec{p},\vec{n}$) reaction at 0° and several beam energies provide empirical evidence that the value of D_{LL} agrees with the energy dependence of the $\Delta S=1$ part of the free *NN* amplitudes. A summary of the values of the polarization observables for all the targets studied in this experiment is presented in Table II. In addition, we indicate the fraction of the cross section that is expected to be $\Delta S=1$ and $\Delta S=0$ as determined from this complete set of polarization observables. These observables are also given for the *NN* charge exchange reaction as determined from the SAID *NN* phase shift amplitudes [37] at 200 and 795 MeV. We do not have polarization data for the Pb(p,n) reaction at 200 MeV; however, D_{NN} for this reaction at 135 MeV have been reported [38].

The GT excitation is an ($\Delta L=0$, $\Delta S=1$) unnatural parity excitation and the spin decomposition analysis confirms that unnatural parity strength dominates the region which is known to be at 0°, predominantly GT. The region of the broad resonance (excess cross section) is also spin flip and if this region is dominated by $\Delta L=0$ strength, this region is also of spin-unnatural parity character. We assume this region is dominated by $\Delta L=0$ because at 800 MeV the momentum transfer (q) is relatively small even at high excitation energy (ω) in contrast to data taken at lower energies.

TABLE III. In this table are the values for the fractional contribution of each partial cross for the $\Delta S=1$ part of the cross section. The symbol $I_{\Delta S=1}$ denotes the sum of the two transverse and spin-longitudinal cross sections that make up the $\Delta S=1$ cross section. The fraction of the cross section that is $\Delta S=0$ is provided in Table II.

Target	$I_p/I_{\Delta S=1}$	$I_n/I_{\Delta S=1}$	$I_q/I_{\Delta S=1}$
^{2}H	0.440±0.019	0.440±0.019	0.119±0.011
C(g.s.)	0.471±0.014	0.471±0.014	0.077±0.017
Pb(0–20)	0.462±0.013	0.462±0.013	0.075±0.018
Pb(20–55)	0.453±0.009	0.453±0.009	0.094±0.008
NN(795)	0.447	0.447	0.105
NN(200)	0.317	0.317	0.366

For example, for the 795 MeV data, near the center of the resonance ($\omega=36$ MeV) the momentum transfer is quite small ($q=0.21$ fm^{-1}). In addition, the angular acceptance of the detector is very small (0.29°) and we do not expect strength from higher ΔL transitions to contribute.

The dominance of the spin-transverse part of the cross section compared to the spin-longitudinal part in the Pb data is indicative of a strong exchange tensor component in the reaction [32]. This is also evident in the ^{2}H polarization transfer data which are representative of the free *NN* interaction. In Table III, the decomposition of the spin part of the cross section is presented integrated over the low and over the high excitation regions. The fractional contribution of the spin-longitudinal and spin-transverse parts are shown along with the decomposition for the free *NN* interaction. We note that the spin-transverse part is slightly larger for the Pb$(\vec{p},\vec{n})$ and C$(\vec{p},\vec{n})$ reaction data than for the ^{2}H$(\vec{p},\vec{n})$ data. The spin-longitudinal part of the cross section is correspondingly smaller for the data taken on the Pb and C targets compared to ^{2}H. It is possible that the differences observed between these channels for data taken on ^{2}H compared to the data taken on the heavier targets is a result of the medium modification of the spin-dependent interaction that was observed in Ref. [32].

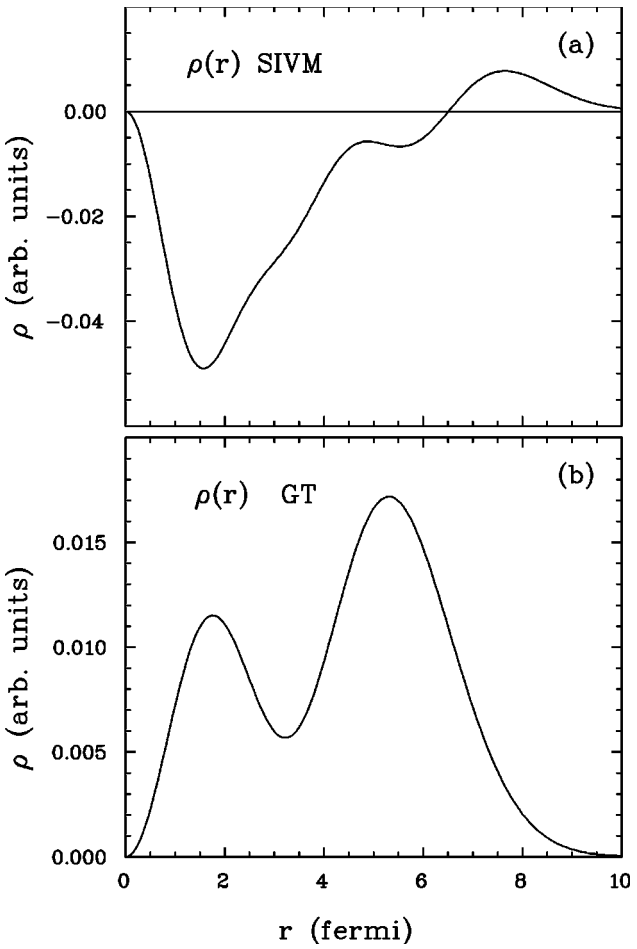

FIG. 4. In the top panel is shown the radial transition density for the SIVM resonance for Pb formed by folding harmonic oscillator wave functions assuming simple shell model configurations. In the bottom panel the transition density for the GT transition is shown. The node at the nuclear surface for the SIVM can be seen. When the transition density is weighted by r^2 and integrated the contributions from the two lobes cancel. This represents what will occur with a probe that samples the full nuclear volume. This cancellation will not occur with a surface probe, resulting in a larger cross section compared to the cross section from a volume probe. This phenomenon is absent in the case of the GT transition since there is no node in the transition density.

IV. THEORY

A. Overview

We summarize the argument advanced by Auerbach [13,14] regarding the excitation of the isovector monopole using the (p,n) reaction. The IVM and SIVM resonances are excited by the operators: $Q_{00}=\Sigma_i r_i^2\tau_i$ and $Q_{01}=\Sigma_i r_i^2\sigma_i\tau_i$. These operators connect, without a change in angular momentum, $(\Delta L=0)$, states that differ by $2\hbar\omega$. The radial transition density formed by folding these states together has a single node near the surface of the nucleus [13]. If the nuclear excitation is done with a probe that penetrates the nuclear interior, the inner and outer lobes of the transition density contribute coherently and will essentially cancel each other resulting in a very small differential cross section. However, if the nuclear probe is attenuated in the nuclear medium the contribution of the innerlobe will be diminished with respect to the outer one preventing the cancellation. The greater the nuclear attenuation of the incident probe, the less contribution from the inner lobe which leads to a greater cross section for the monopole excitation. The degree of attenuation of protons in nuclei is energy dependent and is commonly represented in terms of a distortion factor. At 795 MeV the distortions for the (p,n) reaction become quite large compared to those at 200 MeV. Therefore, the cross section due to the monopole is expected to be greater at the higher energy.

Shown in the top panel of Fig. 4 is the radial transition density for the spin-isovector-monopole resonance. It was obtained from folding together harmonic oscillator wave functions assuming particle-hole states from a simple shell model for $2\hbar\omega$ transitions [39] and shows the node close to the nuclear surface. This is in contrast with the radial transi-

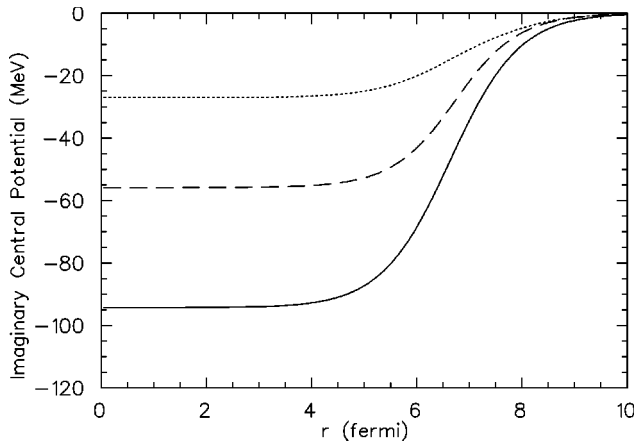

FIG. 5. Shown is the imaginary part of the optical potential for 200 (dotted), 500 (dash-dotted), and 800 (solid) MeV. The strength of the optical potential at 800 MeV causes inelastic nucleon-nucleus reactions to become very surface peaked.

tion density for the GT transition density shown for comparison in the bottom panel of Fig. 4.

The degree of attenuation of the incoming probe is determined by the distortion factor which can be observed through the imaginary part of the optical model potential. The deeper this potential is, the larger the absorption will be resulting in attenuation of the incoming probe. In Fig. 5 we plot the imaginary part of the optical model potentials that will be used in the DWIA calculations below. The 800 MeV potential is almost twice as deep as that of the 200-MeV potential indicating we should expect greater attenuation of the probe at 795 MeV. The energy dependence of the distortion factor and the effect on the attenuation of protons has been noted previously [40].

B. DWIA calculations

We have performed detailed distorted-wave-impulse-approximation (DWIA) calculations for the SIVM resonance at incident energies of 200, 500, and 800 MeV, using the distorted wave code DW81 [41]. Three main ingredients are needed for these calculations, the first being the optical model potential (OMP) parameters. We have incorporated the relativistic optical model potentials in the Schrodinger equivalent form from [42] at all energies. This method gives us a consistent energy dependence for the OMP. The second ingredient is the interaction between the incident and struck nucleon. The free nucleon-nucleon interaction as parametrized by Franey and Love [43], was used in these calculations. In a few cases and where available a comparison of the results was done with calculations using a new version [44] of these interactions. No major differences between the two calculations were observed. The third ingredient needed in the DWIA calculations is a one-body density transition matrix element. We used particle-hole transition strengths from a simple collective model NORMOD [39], which includes particle-hole $2\hbar\omega$ transitions for the corresponding sub shells. The code predicts that the SIVM strength increases dramatically with increasing atomic number (A), due to the increase in the number of particle-holes available. Thus for

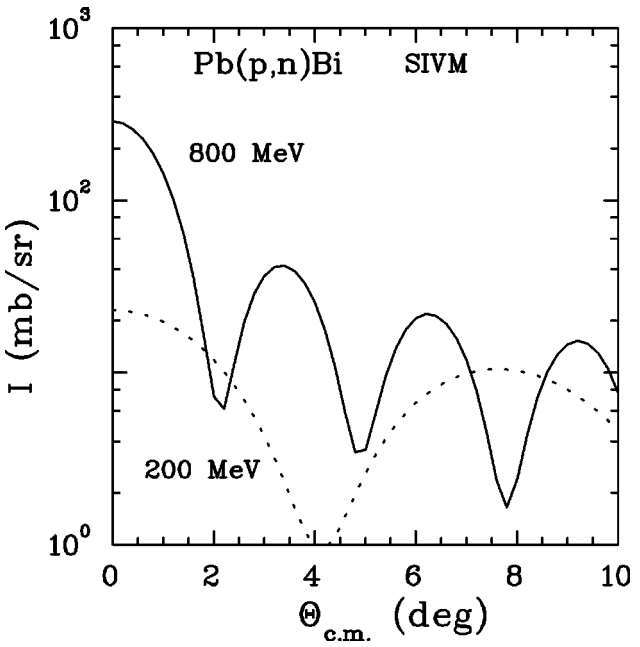

FIG. 6. Shown are the results of DWIA calculations of the angular distribution of the center-of-mass differential cross section for the SIVM resonance in the ^{208}Pb(p,n) reaction, assumed to be located at 32 MeV excitation. The solid line is the result for an incident proton energy of 800 MeV and the dashed line is for 200 MeV.

^{12}C a SIVM strength of 16.3 fm^4 is evaluated, for ^{90}Zr 983 fm^4 and for ^{208}Pb 6688 fm^4. This explains the results shown in Fig. 1, where essentially there is no excess of cross section in the resonance region for ^{12}C while the excess is larger for ^{208}Pb than for ^{90}Zr.

In Fig. 6 we present the forward angle angular distribution calculated for the ^{208}Pb(p,n)^{208}Bi (32 MeV) SIVM transition at 200 and 800 MeV. In Fig. 7, we present zero degree differential cross sections as a function of bombarding energy calculated for the same reaction but for different transitions. The SIVM at 32 MeV of excitation is presented with a solid line, the giant GT resonance at 15.6 MeV excitation with a dot-dashed line and the Fermi transition at an excitation energy of 15.3 MeV with a dashed line. The calculations indicate an increase by a factor of 13 for the SIVM zero degree cross section at 800 MeV compared with that at 200 MeV which we attribute to the arguments presented in the previous section. The zero degree differential cross section calculations for the GT transition indicate a rather constant value with incident proton energy. The Fermi transition indicates an increase in the zero degree cross section by a factor of about 3 at 800 MeV compared with the calculation done at 200 MeV. We also have calculated the $\Delta L=2$, $\Delta S=1$, $\Delta J=1$ contribution to the SIVM. At lower energies the contribution is rather small, 1–2 % of the $\Delta L=0$, $\Delta S=1$, $\Delta J=1$ main contribution, but at 800 MeV and due to the tensor interaction both in the direct and exchange terms, the $\Delta L=2$ contribution increases to about 40% of the $\Delta L=0$ contribution. However, the $\Delta L=2$, $\Delta S=1$ calculation indicates a large and negative D_{NN} and a large positive D_{LL},

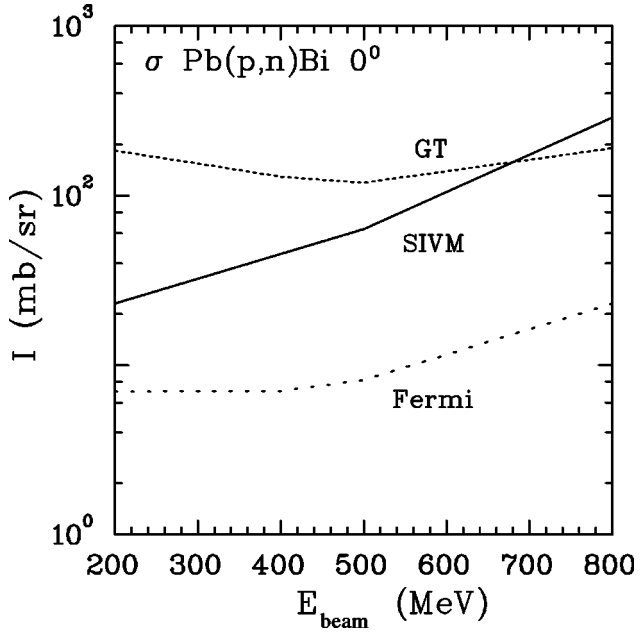

FIG. 7. The figure shows results for calculations of the energy dependence of the 0° center-of-mass differential cross section for the ^{208}Pb(p,n) reaction. The SIVM resonance is shown as a solid line, the GT transition as a dot-dashed line, and the Fermi transition as a dashed line.

values which are not in agreement with the empirical results. In the region of the SIVM (see Table II), the present results are $D_{NN}=0.014\pm0.013$ and $D_{LL}=-0.637\pm0.012$. The $\Delta L=0$, $\Delta S=1$ SIVM calculated values are $D_{NN}=-0.265$ and $D_{LL}=-0.47$, in better agreement with data. Since the $\Delta L=2$, $\Delta S=1$ calculations depend strongly on the tensor interaction, it would be important to recalculate these values when a new 800-MeV interaction becomes available [44].

In all the above DWIA calculations, the SIVM resonance was assumed to be at an excitation energy of 32 MeV which is where the data from the experiment appear to peak. In fact, this resonance is quite broad, about 25 MeV FWHM, and the *NN* interaction could change over this excitation range affecting the magnitude of the cross section of the resonance. To include this effect, we have performed a ''folding'' calculation. The DWIA calculation for the SIVM was performed at each excitation energy bin spanning the width of the resonance. The calculations were done for each 4 MeV bin between 22 and 62 MeV. Each bin represents a fraction of the SIVM cross section. This fraction was determined for each bin from the empirical cross section shown in Fig. 2, since we assume this gives a good indication of the shape of the resonance. The DWIA calculations were then weighted by this fraction and the result summed to obtained a weighted average of the SIVM cross section. The result obtained was 260 mb/sr and is about 11% lower than the cross section obtained assuming the SIVM resonance is located at 32 MeV of excitation energy as shown in Figs. 6 and 7.

The response function for the SIVM has been calculated by Auerbach and Klein in the random phase approximation (RPA) [45]. They report the peak of the resonance at 42.5 MeV with a nominal width of 12.5 MeV FWHM. A plot of the response function is presented in Ref. [45] and indicates the strength for the resonance is spread over a region of excitation from 20 to 60 MeV similar to the shape of our data in Fig. 2. Recent detailed calculations for the SIVM have shown the resonance peaked at a lower energy, 36.9 MeV, in closer agreement to our data [46,47].

Full detailed calculations of cross sections and PT observables for the excitation spectrum of these reactions are needed. In addition, experimental cross section data and PT observables for the Pb$(\vec{p},\vec{n})$ reaction at 795 MeV at several angles would allow a multipole decomposition of spin and nonspin components of the excitation spectrum for this reaction. Such data are needed to provide a solid indication of the multipolarity of the excess cross section in the high excitation region of the spectrum.

V. SUMMARY

We have presented the first complete polarization decomposition of the giant resonance region at 0° using the Pb$(\vec{p},\vec{n})$ reaction at 795 MeV. We have compared our cross section results to the same reaction at 200 MeV and found an excess cross section in the 795-MeV data that is broadly distributed about an excitation energy of 32 MeV. Results of DWIA calculations for the spin isovector monopole resonance are also presented. We surmise that the large cross section observed at around 32 MeV in the Pb(p,n) reaction results from excitation of the spin isovector monopole resonance (SIVM). This is based on three observations: (1) The ratio of the cross section in this high excitation region with that in the low excitation ''GT'' region is dramatically increased when compared to this ratio for the same reaction at 200 MeV, consistent with expectations based on the decrease in the nuclear transparency at the higher energy compared to that at 200 MeV. This trend is also borne out from results of DWIA cross section calculations done for this resonance at 200 and 800 MeV. (2) The polarization transfer observables at 795 MeV may be used to project out the spin part of the cross section. The projection indicates this region is almost entirely spinflip ($\Delta S=1$) similar to the low excitation GT region of the spectrum. The DWIA results for the PT observables are also consistent with the data. Results of calculations of a possible $\Delta L=2$, $\Delta S=1$ resonance that could contribute at 0° are in disagreement with the PT observable data. (3) At 795 MeV this extra cross section is only seen in reactions on heavier targets such as Zr and Pb and is absent in light targets such as ^{12}C. This observation is consistent with the DWIA calculations that indicate many more particle-hole configurations contribute to the SIVM resonance in reactions on the heavy nuclei then on light nuclei. The present results are in complete agreement with the observations by Auerbach [13] about the nature of the excitation of this SIVM resonance.

ACKNOWLEDGMENTS

We would like to thank S.Y. van der Werf and Nils Olsen for providing us the code NORMOD. This work was supported in part by the U.S. DOE and NSF.

[1] T.N. Taddeucci *et al.*, Nucl. Phys. **A469**, 125 (1987).
[2] G.F. Bertsch and H. Esbensen, Rep. Prog. Phys. **50**, 607 (1987).
[3] F. Osterfeld, Rev. Mod. Phys. **64**, 491 (1992).
[4] X. Yang *et al.*, Phys. Rev. C **52**, 2535 (1995).
[5] N. Auerbach, F. Osterfeld, and T. Udagawa, Phys. Lett. B **219**, 184 (1989).
[6] D.M. Youngblood, Y.-W. Lui, and H.L. Clark, Phys. Rev. C **60**, 014304 (1999), and references therein.
[7] N. Auerbach (private communication).
[8] J.D. Bowman *et al.*, Phys. Rev. Lett. **50**, 1195 (1983); A. Erell *et al.*, Phys. Rev. C **34**, 1822 (1986).
[9] S. Nakayama *et al.*, Phys. Rev. Lett. **83**, 690 (1999).
[10] M. Moinester *et al.*, Phys. Lett. B **230**, 41 (1989).
[11] R.G.T. Zegers *et al.*, Phys. Rev. Lett. **84**, 3779 (2000).
[12] A. Brockstedt *et al.*, Nucl. Phys. **A530**, 571 (1991).
[13] N. Auerbach, Comments Nucl. Part. Phys. **32**, 223 (1998).
[14] N. Auerbach *et al.*, Phys. Rev. C **28**, 280 (1983).
[15] P.M. Boucher and B. Castel, Phys. Rev. C **40**, 2897 (1989).
[16] X.Y. Chen *et al.*, Phys. Rev. C **47**, 2159 (1993).
[17] T.N. Taddeucci *et al.*, Phys. Rev. C **41**, 2548 (1990).
[18] D.L. Prout *et al.*, Phys. Rev. C **52**, 228 (1995).
[19] J. Rapaport *et al.*, Phys. Rev. C **36**, 500 (1987).
[20] C.D. Goodman *et al.*, Phys. Rev. Lett. **54**, 877 (1985).
[21] C. Gaarde *et al.*, Nucl. Phys. **A369**, 258 (1981).
[22] F. Osterfeld, D. Cha, and J. Speth, Phys. Rev. C **31**, 372 (1985).
[23] D. Cha and F. Osterfeld, Phys. Rev. C **39**, 694 (1989).
[24] J. Rapaport and E. Sugarbaker, Annu. Rev. Nucl. Part. Sci. **44**, 109 (1994).
[25] J. Rapaport *et al.*, Phys. Rev. C **39**, 1929 (1989).
[26] E. Sugarbaker *et al.*, Phys. Rev. Lett. **65**, 551 (1990).
[27] T.N. Taddeucci *et al.*, Phys. Rev. C **42**, 935 (1990).
[28] A. Klein and W.G. Love, Phys. Rev. C **33**, 1920 (1986).
[29] R. Jeppesen, Ph.D. dissertation, University of Colorado, 1986.
[30] T. Wakasa *et al.*, Phys. Rev. C **55**, 2909 (1997).
[31] M. Ichimura and K. Kawahigashi, Phys. Rev. C **45**, 1822 (1992); **46**, 2117 (1992).
[32] D.J. Mercer *et al.*, Phys. Rev. Lett. **71**, 684 (1993).
[33] T. Wakasa *et al.*, Phys. Rev. C **51**, R2871 (1995).
[34] T.N. Taddeucci *et al.*, Phys. Rev. C **33**, 746 (1986).
[35] H. Sakai *et al.*, Phys. Rev. C **35**, 344 (1987).
[36] B.D. Anderson *et al.*, Phys. Rev. C **54**, 1531 (1996).
[37] R.A. Arndt and L.D. Roper, Scattering Analyses Interactive Dial-In Program (SAID), Virginia Polytechnic Institute and State University (unpublished).
[38] M.R. Plumley *et al.*, Phys. Rev. C **56**, 263 (1997).
[39] S.Y. van der Werf (private comunication); M.A. Hofstee *et al.*, Nucl. Phys. **A588**, 729 (1995).
[40] R.D. Smith and M. Bozonian, Phys. Rev. C **39**, 1751 (1989).
[41] R. Schaeffer and J. Raynal, computer code DWBA70 (unpublished); J.R. Comfort, extended version DW81 (unpublished).
[42] S. Hama, B.C. Clark, E.D. Cooper, H.S. Sherif, and R.L. Mercer, Phys. Rev. C **41**, 2737 (1990).
[43] M.A. Franey and W.G. Love, Phys. Rev. C **31**, 488 (1985).
[44] W.G. Love (private communication).
[45] N. Auerbach and A. Klein, Phys. Rev. C **30**, 1032 (1984).
[46] V.A. Rodin and M.H. Urin (unpublished).
[47] M. Urin (private communication).